PHENOMENOLOGICAL INVESTIGATIONS ON THE TURBULENT FLOW STRUCTURES IN A ROD BUNDLE ARRAY WITH MIXING DEVICES

Seok Kyu Chang[a,b], Sang Ki Moon[a], Bok Deuk Kim[a], Won Pil Baek[a] and Young Don Choi[b]

[a] Korea Atomic Energy Research Institute, 105, Dukjin-Dong, Yusong-Ku, Daejon, 305-353, Republic of Korea, skchang@kaeri.re.kr, skmoon@kaeri.re.kr, bdkim@kaeri.re.kr, wpbaek@kaeri.re.kr

[b] Korea Univ., Mechanical Engineering Dept., 1, 5Ka, Anam-Dong, Sungbuk-Ku, Seoul, Republic of Korea, ydchoi@korea.ac.kr

Abstract

Detailed turbulent flow profiles have been measured on a square sub-channel geometry with typical mixing devices. For a fine examination of the lateral flow structure on a sub-channel geometry with 2-D LDA, a 5x5 rod bundle array was fabricated as 2.6 times larger than the real bundle size. The mixing devices used were a typical split type and a swirl type. The experiments were performed at the condition of Re=50,000 (axial bulk velocity 1.5 m/s) and the water loop was maintained at the conditions of 35 ºC and 1.5 bar during an operation. As for the results, distinct intrinsic flow features were observed according to the type of mixing devices. In a typical split type, there was no remarkable swirling flow within a sub-channel and the lateral flow was vigorous in the gaps. In the swirl type, a single swirling flow was dominant within a sub-channel and there were relatively small lateral flows in the gaps.

Introduction

In a nuclear power plant, an optimum heat removal from the surface of the nuclear fuel elements in a reactor is very important for the viewpoint of a reactor thermal margin and safety. The spacer grids which support the fuel assembly are used as the effective thermal mixing devices by attaching various types of flow deflectors. There are many efforts being made to develop the optimum spacer grid which can mix the flow effectively in sub-channel geometry. Recently, due to the great advances in computation technology, commercial CFD codes are being used to design the optimized flow mixing device. However, no CFD code is still successfully available for an estimation of the flow structure in this geometric condition because of the complexity of the flow and the severe anisotropy of the turbulent diffusion. There have been many attempts to improve the calculation performance of the CFD code by improving the turbulence model and the numerical schemes. The verification of the CFD code by comparing it with experimental data is essential prior to an application. But the experimental data of the flow structure caused by a mixing device on sub-channel geometry is very limited for a satisfiable verification of the developed computational tools. Even from the available experimental data, they are not enough to examine the small scales of the lateral flow generated by a mixing device. From this reason, more precise experimental studies are required to use for the code verifications.

There have been many efforts to find the mechanism of a thermal mixing in a structure comprised of many regular arrayed rods. Trupp and Azad [1] inferred the existence of a secondary flow in a sub-channel from the measurements of the axial velocity profile and the shear stress of the rod surfaces. Neti et. Al. [2] and Vonka [3] tried to measure the lateral velocity profiles within sub-channels by using 2-D LDA and they confirmed that the magnitudes were less than 1 % of the averaged axial velocity but detailed secondary flow features were unclear. Rowe et. Al. [4] suggested the existence of a lateral macro-scale from the measurements of the dominance frequency of turbulence in a square sub-channel geometry. Rehme [5] confirmed the lateral flow pulsations between the sub-channels by analyzing the space cross-correlations of the HWA measurements. He insisted that the thermal mixing in a sub-channel geometry is mostly influenced by the almost periodic macro-scale flow pulsations caused by the flow instability rather than the secondary flow from the Reynolds stress gradients. There also have been many studies on a thermal hydraulic analysis of the sub-channel geometry. These studies agreed with the experimental data to some degree by using different turbulence models but none could simulate the lateral flow pulsations.

Yang and Chung [6] have studied the influence of the spacer grids on the turbulent mixing within a square sub-channel geometry. They analyzed the generation and decay of the turbulent energy from their LDA measurement results. Karoutas et. Al. [7] have performed an analysis of the fluid dynamics under the influence of spacer grids in a square sub-channel geometry. They compared the calculations with their experimental results and showed good agreements for the lateral velocity profiles. But the axial velocity comparison had some differences because of the assumption of an infinitesimal vane thickness in the calculation. Smith et. Al. [8] have demonstrated a process used to develop confidence in CFD as a tool to investigate the flow and temperature distributions in a rod bundle array with spacer grids. They performed thermal hydraulic experiments in a 5x5 rod bundle array with mixing vanes by using the PIV system and a heater rod. CFD simulation was also performed with the same conditions as the experiments. The CFD predictions showed reasonable agreements with the data for the velocity fields and the rod heat transfer coefficients.

This study presents the experimental data of the detailed turbulent flow structures on a square sub-channel geometry with typical mixing devices. The measurement results show the inherent flow characteristics for each type of spacer grid according to the configuration of the mixing vanes.

It is expected that the information of these flow characteristics in sub-channels can be used for the verifications of related CFD codes. And these experimental results would also be useful for developing optimized fuel rod components.

Experimental Apparatus

The experiments have been conducted in the cold test loop at KAERI which can perform the hydraulic test at normal pressure and temperature conditions for a rod bundle array in water. Figure 1 shows the schematic of the cold test loop used in this work. It consists of a water storage tank, circulation pump and a test section. A heater and cooler are installed in the water storage tank for maintaining the experimental temperature condition during an operation. Coolant flow rate is controlled by changing the pump speed with an inverter at up to 2 m^3/min..

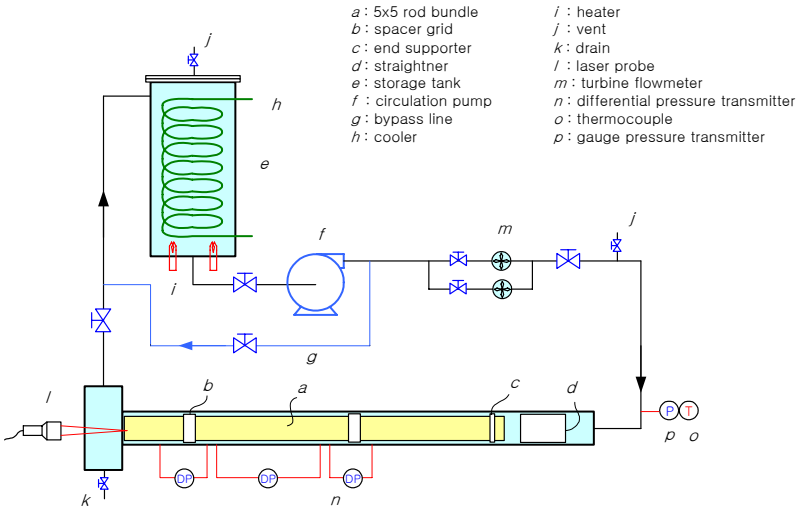

Figure 1. Schematic diagram of the experimental apparatus

There are several instruments to monitor and control the loop conditions. The measured temperature from the thermocouple at the water storage tank is used to control the heater and the control valve at the cooling line for maintaining the loop temperature. Pressure transmitters are installed to measure the loop pressure and the local differential pressures in the test section. To measure a wide range of the flow rates, two turbine type flow-meters are used. One is for a low flow rate (0.5~8.2kg/s), and the other is for a higher flow rate (2.5~40.9 kg/s). The experimental data of the loop is collected by using a data acquisition unit (Agilent 34970A).

LDA System

A 2-component Laser Doppler Anemometry (LDA) was used to measure the turbulent velocities in a rod bundle. It comprises of an Argon-ion Laser source, optics and a 2-D probe. We employed the **FiberFlow optics/transmitter** of DANTEC* which uses a backward scattered method as an optical system of this 2-dimensional LDA. Figure 2 shows the features of the LDA system schematically. Although the signal can be obtained in ordinary water, for more signals, seeding particles of hollow

* Dantec Measurement Technology,
http://www.dantecmt.dk/LDA/System/Index.html

glass spheres with a diameter of 10 μm were added into the water. The focal length of the lens, F is 310 mm and the beam expander ratio, E is 1.0. The diameter, D_L and the spacing, D of the beam are 1.35 mm and 24 mm, respectively. The 2-D laser beams have a wavelength of 514.5 nm for the green color and 488 nm for the blue color. Measurements are made at the intersection between the two incident laser beams. The measurement volume is an ellipsoidal shape whose height δ_x, width δ_y, and length δ_z are 0.15, 0.15, and 3.54 mm, respectively. And it determines the spatial resolution and the accuracy of the measurement.

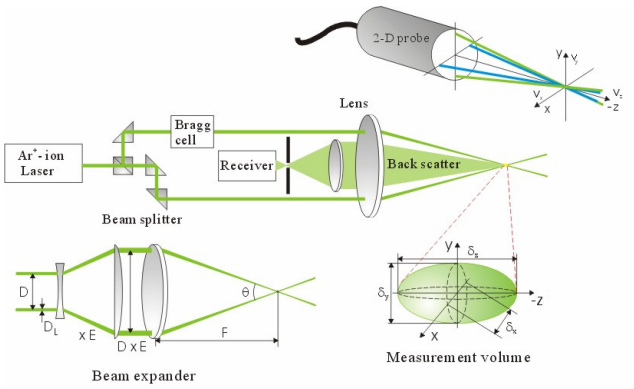

Figure 2. Schematic diagram of the principle of the LDA system

Test Section

For a close examination of the lateral flow structure on a sub-channel geometry, a 5x5 rod bundle array was fabricated as 2.6 times larger than the real bundle size. This 5x5 rod bundle with spacer grids was installed in the acrylic square duct. Both ends of the rod bundle were fixed with the support grids of which the strap was thin enough to minimize the flow disturbance. The support grid for one end of the rods at the downstream side was especially designed to allow for a laser beam passing. The LDA measurements were performed at the plane 5 mm inside the end of the rods at the downstream side. The cones were attached to the ends of the rods at the downstream side to minimize the vortices behind the ends of the rods which could make a flow deformation at the measurement locations.

Two spacer grids were assembled to the 5x5 rod bundle array. The first spacer grid which is placed at the upstream of the test section has no mixing devices and is for a stabilization of the flow. The second spacer grid is placed at 70 D_h apart from the first spacer grid in the direction of the downstream. This second spacer grid has mixing devices and it causes a lateral mixing and/or a swirling flow. A set of spacer grids can be moved along the axial direction according to the test conditions. The total channel length and the grid span are 4900 and 1700 mm, respectively.

The 2-D LDA was positioned in front of the main flow cross section of the 5x5 rod bundle array for measuring the lateral velocity vectors on every point in a flow sub-channel. The axial velocity component was also measured by changing the location of the LDA probe to the side of the test section.

Figure 3 describes the cross-sectional configuration of the test section and the LDA investigation region. The size of the inner square of the test section is 170×170 mm. The geometric configurations of the bundle array are rod dia., $D = 25.4$ mm, rod pitch, $P = 33.12$ mm and wall pitch, $S = 18.76$ mm, respectively. Hydraulic diameter $D_h = 24.27$ mm is evaluated from considering the whole effective flow

area and wetted perimeter within the square duct with a 5x5 rod bundle. The LDA investigation region enclosed by a dotted line is comprised of three kinds of sub-channel: inner, intermediate and wall sub-channel. Measuring points are closely distributed with resolutions of 0.75 mm for precise examination of the lateral flow distribution in the sub-channels.

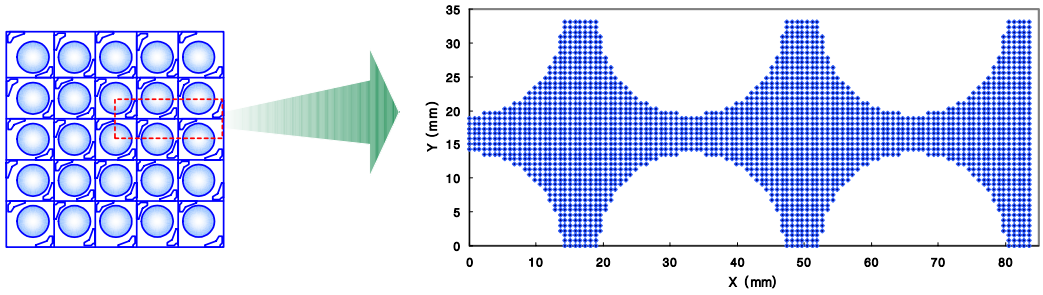

Figure 3. Cross-sectional configuration of the test section and the investigating region

The mixing devices used in this study were a typical split type and a swirl type. Figure 4 shows the schematic of the mixing devices. The split type is considered to enhance the flow mixing between the sub-channels vigorously through the gaps. Meanwhile, the swirl type makes a strong vortex which can disperse the thermal energy within a sub-channel rather than a flow interchanging between the sub-channels. The swirl type has a pair of primary vanes (bigger) and a pair of secondary vanes (smaller) in a sub-channel.

(a) Split type (b) Swirl type

Figure 4. Mixing devices tested in this work

Results and Discussion

The measurements for the lateral velocities at the investigation region were performed at 2,412 positions as shown in Figure 3. The measurements for the axial velocities were only available at the horizontal rod gap because of an interruption of the beam crossing due to the rods. 770 positions were measured for the axial velocities in the rod gap. The number of samples for each measurement was about 5,000 and it took about 20 seconds per one measurement. The measuring cross sections lay at 1 D_h, 2 D_h, 4 D_h, 8 D_h and 16 D_h apart from the end of the test spacer grid. The experiments were performed at the condition of Re=50,000 (axial bulk velocity 1.5 m/sec.) in the test section and the water loop was maintained at the conditions of 35 ºC and 1.5 bar during an operation.

Flow Features

Figure 5 shows the LDA measurement result of the lateral velocity vectors in the investigation region for two types of the spacer grid at the level of 1 D_h apart from the tip of the mixing vanes.

Three sub-channels in each case ((a),(b)) are the inner (left), intermediate (center) and wall (right) sub-channel, respectively. The velocity profiles are differentiated between the types of the spacer grid according to the configurations of the mixing devices.

In case (a) for the split type, there is a couple of symmetric vortices generated by the split vanes within a sub-channel at the inner and intermediate sub-channels. The size of each vortex is about one forth of a pitch. These localized small vortices contribute to a thermal mixing in a very limited region within a sub-channel. The cross-flow at four gaps in a sub-channel is vigorous and mostly contributes to the energy exchange between the adjacent sub-channels. From these, the split type spacer grid is considered to be more effective for a mixing between the sub-channels rather than a mixing within a sub-channel.

Meanwhile, in case (b) for the swirl type, one large vortex of elliptic shape is generated by the swirl vanes within a sub-channel at the inner and intermediate sub-channels. The size of the vortex is about 2.6 times larger than that of case (a). This large swirling flow makes flatten the temperature profile caused by the heat flux from the fuel rod surfaces in a sub-channel. There is also a cross-flow at four gaps which is effective for the mixing between the sub-channels but the contribution of the inter-channel mixing is less than that of case (a). Thus the swirl type has a better performance for a thermal mixing within a sub-channel while it has a lesser contribution for a inter-channel mixing when compared to the split type. The magnitudes of the lateral peak velocities in this investigation region are about 30% of the axial bulk velocity (1.5 m/s) in both cases.

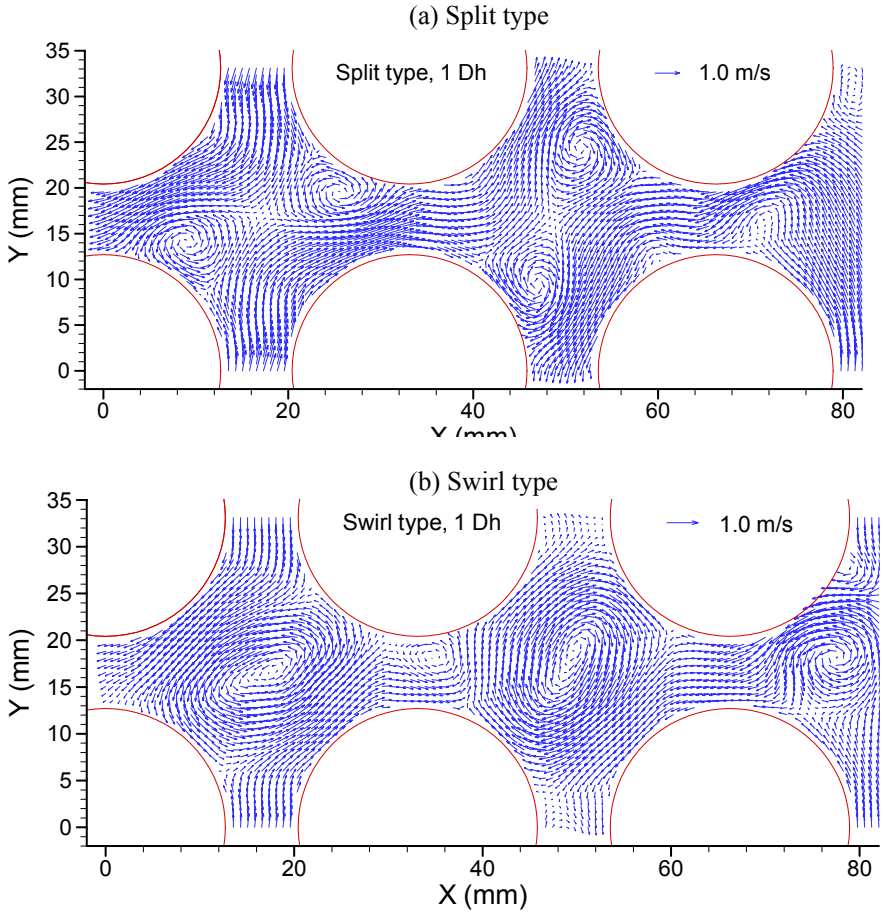

Figure 5. Lateral velocity vectors

Figure 6 shows the vorticity (ω_z) contour with the velocity vectors at the levels of 1 and 4 D_h for the two types of spacer grid. In case (a) for the split type, a couple of vortices is generated symmetrically according to the vane patterns in a sub-channel at just behind the spacer grid (1 D_h). As a flow passes through the downstream, its strength is weakened and it moves to the rod surface (4 D_h). At a further downstream region, the swirling flow eventually disappears and only a pair of 90° turning cross-flows remain (not shown). In case (b) for a swirl type, one large swirling flow contains two neighboring peaks of vortices in a sub-channel at just behind the spacer grid (1 D_h). As a flow passes through the downstream, vortex peaks are merged into one and the shape of the swirling flow changes to a round pattern from a skewed elliptic form (4 D_h). At a further downstream region, a swirling flow is maintained although the strength is decayed (not shown).

By virtue of the wall effect at the wall sub-channel, there is a relatively large cross-flow through the gap connecting the intermediate sub-channel. This cross-flow skews the flow shape in the intermediate sub-channel and it moves the position of the vortex centre to the left lower region as the flow is passing through the downstream. Thus, the qualitative changes of the flow feature in the intermediate sub-channel which could be caused by the wall effect from the wall sub-channel were not observed.

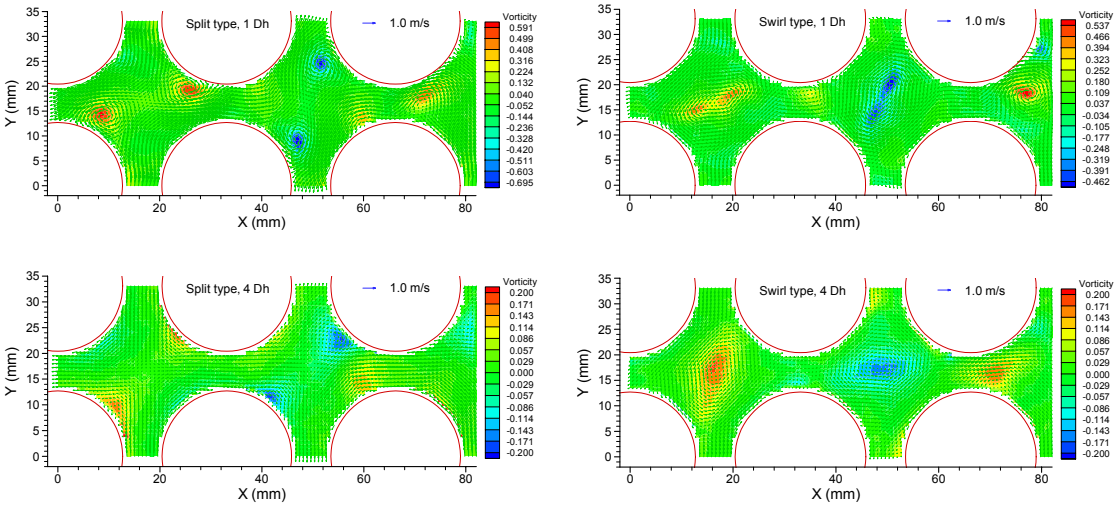

(a) Split type (b) Swirl type

Figure 6. Vorticity contours

Figure 7 shows the comparisons of the axial and lateral velocity profiles between the types of spacer grid along the gap centreline (refer figure 3) as a flow passes through the downstream.

In the left figure, the axial velocity fluctuates in a complicated manner at $z/D_h = 1$ due to the existence of the mixing vanes just upstream. As the flow moves downstream, the velocity fluctuations decrease gradually. At the level of $z/D_h = 16$, the velocity profile of the split type becomes almost flat while the velocity profile of the swirl type shows a wavy form. In the case of the swirl type, the recovery of the flow loss in the wall sub-channel due to the wall and the vaned spacer grid at $z/D_h = 1$ is slower than that in the case of the split type as a flow passes through the downstream. The complete wavy velocity profile at the level of $z/D_h = 71$ is the case of the bare rod bundle experiment for the comparison.

In the right figure, the fluctuations of the lateral velocity profiles in both cases represent the flow characteristics due to the vane patterns, exactly. From the points C1 and C2 at $z/D_h = 1$ which mean the centre of the sub-channels, the symmetric fluctuations in the case of the swirl type allude to a swirling flow (CCW at C1 and CW at C2, respectively), while in the case of the split type they suggest a splitting flow (left/right gaps at C1 and upper/lower gaps at C2, respectively). These features are also confirmed from the examination of the velocity vectors in Figure 5. The lateral fluctuations are decaying gradually as a flow passes through the downstream, but the fluctuations in the case of the swirl type which have a swirling feature remain longer than those in the case of the split type because of the larger vortex scales as discussed above. Also, the almost "zero" profile at the level of the $z/D_h = 71$ is the case of the bare rod bundle experiment for reference.

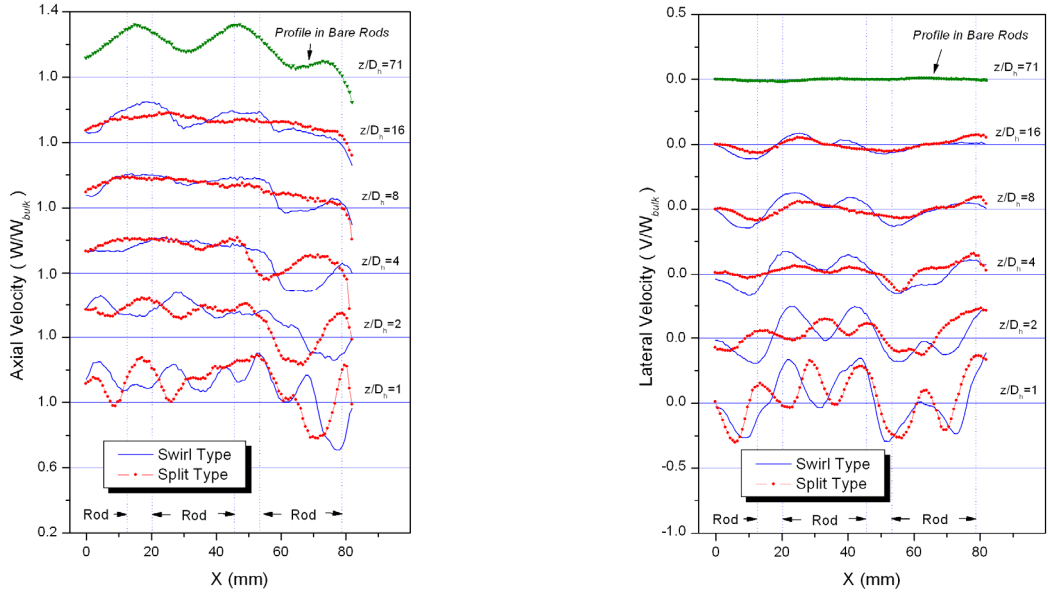

Figure 7. Comparison of the velocity profiles along the gap centerline

Turbulent Intensities

Figure 8 shows the contour of the lateral directional turbulent intensities for the two types at the level of $z = 4\ D_h$. This suggests that there is a distinct relationship between the intensity and the directional patterns of the mixing vanes except for the region lower than $z = 2\ D_h$, where the flow is chaotically redistributed when passing through the mixing devices.

At the inner sub-channel, where there is a mixing device of which the bending direction is horizontal, the turbulent intensity of the V-component (V_{rms}) has relatively large values in a central region, while the turbulent intensity of the U-component (U_{rms}) is not dominant. Meanwhile, at the intermediate sub-channel, where there is another mixing device of which the bending direction is vertical, U_{rms} has relatively large values in a central region, while V_{rms} is not dominant. In the case of the swirl type, the primary vanes of the mixing device play a more important role for determining the pattern of the intensity distribution than the secondary vanes. The turbulent intensity is somewhat larger in the case of the split type than that in the case of the swirl type. The shape of the intensity contour is highly skewed in the case of the swirl type.

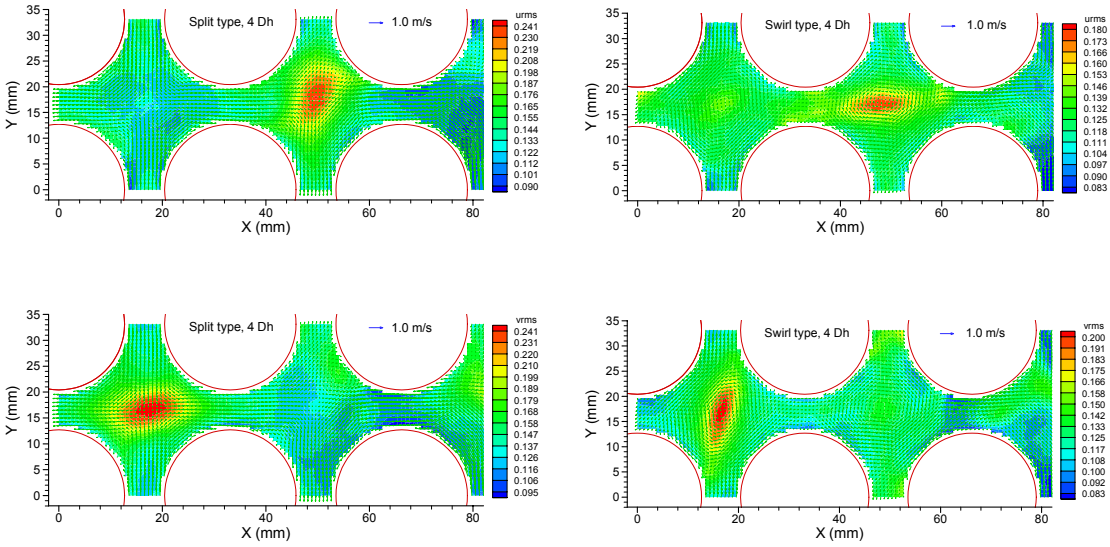

(a) Split type (b) Swirl type

Figure 8. Turbulent intensity contour

Figure 9 shows the turbulent intensity profiles along the gap centreline in the bare rod bundle case. These are normalized with the axial mean velocity for comparisons of the decayed turbulent intensities in the case of the rod bundle with vanes. The axial components are about 4% higher than the lateral components and magnitudes at the centre of the sub-channels are lower than other locations.

Figure 10 shows the decay of the turbulent intensities at various locations in the sub-channels as a flow passes through the downstream for the types of the spacer grids. In all the figures, there are temporal depressions of the turbulent intensity in the sub-channels at just behind the mixing devices (z/D_h =1). These are caused by a chaotic mixing of the flow passing through the spacer grid, where the turbulent fluctuations are irregularly generated in the overall area in the sub-channels at just behind the mixing vanes. As the flow is redistributed (z/D_h > 2), turbulent intensities in the sub-channels are rearranged in an intrinsic manner according to the directional patterns of the mixing vanes.

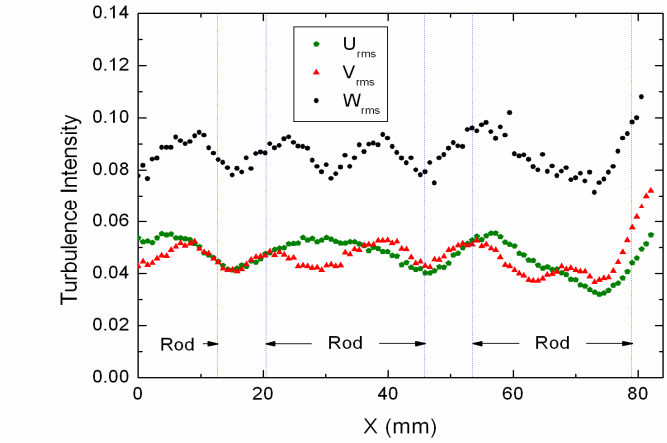

Figure 9. Turbulent intensity profiles in the case of the bare rod bundle along the gap centreline

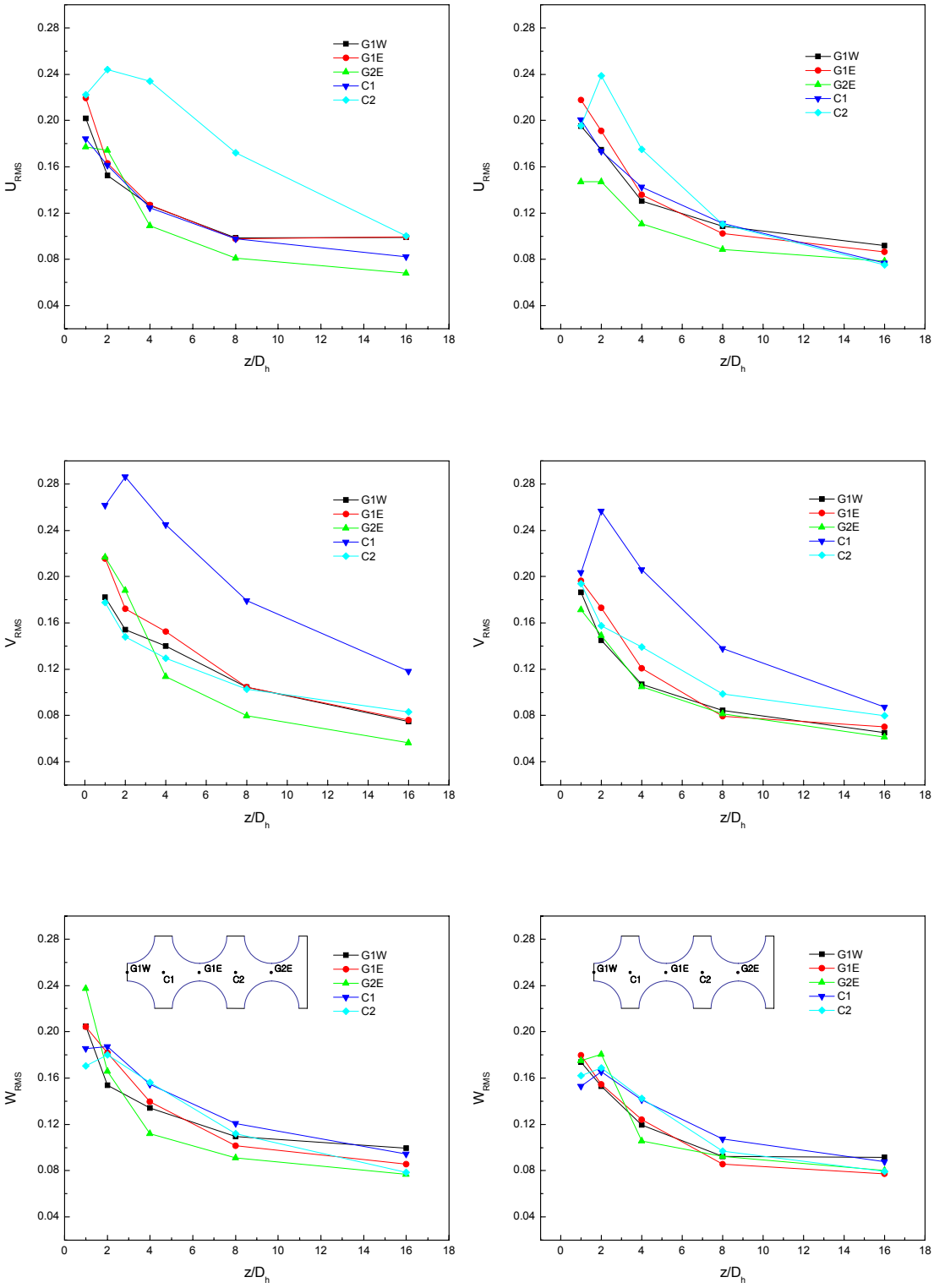

(a) Split type (b) Swirl type

Figure 10. Turbulent intensity decay

In the upper two figures, the U_{rms} at C2 (intermediate sub-channel) is higher than the other locations and in next two figures, the V_{rms} at C1 (inner sub-channel) is higher than the other locations, in the same manner. These imply that there is an obvious dependency between the distributions of the turbulent intensity and the directional patterns of the mixing vanes, as mentioned above.

The differences of the lateral directional turbulent intensities between the maximum and the others are larger in the case of the split type than that in the case of the swirl type. The turbulent intensities are decayed drastically at a close downstream distance from the spacer grid and the decaying rates are decelerated as the flow passes further downstream for both types of the spacer grid.

The turbulent intensity of the W-component (W_{rms}) has no relationship with the directional patterns of the mixing vanes and it is distributed uniformly in the sub-channels. From the results of Figure 10, the split type is somewhat superior to the swirl type in the performance of the turbulence generation at a near downstream distance from the spacer grid.

Conclusions

Detailed turbulent flow profiles have been measured by using 2-D LDA on a square sub-channel geometry with two types of mixing devices. For a fine examination of the lateral flow structure on a sub-channel geometry, a 5x5 rod bundle array was fabricated as 2.6 times larger than the real bundle size. The tested mixing devices were a typical split type and a swirl type. From the experimental results, the characteristics of a turbulent flow in a sub-channel geometry with the specific mixing devices are summarized as follows.

In the case of the split type, a couple of symmetric small vortices were generated in a sub-channel just after the split vanes and it disappeared as the flow moves downstream while the cross-flow at four gaps in a sub-channel was vigorous. The split type spacer grid is considered to be more effective for a mixing between neighboring sub-channels rather than a mixing within a sub-channel.

In the case of the swirl type, one large vortex of an elliptic shape was generated in a sub-channel just after the split vanes and it was maintained until the flow moves downstream. The cross-flow at four gaps in a sub-channel was relatively weak. The swirl type has a better performance for a thermal mixing within a sub-channel when compared to the split type.

The bending direction of the mixing vanes influences the turbulence generation in such a way that the component of the turbulent intensity perpendicular to the vending direction is dominant in a sub-channel.

The turbulent intensity in the case of the split type is larger than that in the case of the swirl type at just behind the mixing devices, but it decays exponentially in both cases in a similar way as the flow moves to the downstream.

The experimental results from this work would be useful for the development of a turbulence model for applications such as sub-channel geometries, where the flow is highly non-isotropic, and also for a verification of the reactor analysis CFD codes.

Nomenclature

D	rod diameter, mm
D_h	hydraulic diameter, mm
D_L	beam waist diameter before passing the front lens, mm
E	beam expansion ratio, -
F	focal length of the front lens, mm
P	rod pitch, mm
Re	Reynolds number ($\rho W_{avg} D_h / \mu$), -
S	wall to rod pitch, mm
u	lateral fluctuating velocity in the x-direction, $m/\sec$
U	lateral time mean velocity in the x-direction, $m/\sec$
U_{rms}	relative lateral turbulence intensity in the x-direction ($U_{rms} = \frac{\sqrt{u^2}}{W_{avg}}$), -
v	lateral fluctuating velocity in the y-direction, $m/\sec$
V	lateral time mean velocity in the y-direction, $m/\sec$
V_{rms}	relative lateral turbulence intensity in the y-direction ($V_{rms} = \frac{\sqrt{v^2}}{W_{avg}}$), -
w	axial fluctuating velocity in the z-direction, $m/\sec$
W	axial time mean velocity in the z-direction, $m/\sec$
W_{avg}	axial average or bulk velocity through a rod bundle in the z-direction, $m/\sec$
W_{rms}	relative axial turbulence intensity in the z-direction ($W_{rms} = \frac{\sqrt{w^2}}{W_{avg}}$), -
x	coordinate in depth, mm
y	vertical coordinate, mm
z	axial coordinate, mm
δ_x	x-size of the measurement volume of the laser beam, mm
δ_y	y-size of the measurement volume of the laser beam, mm
δ_z	z-size of the measurement volume of the laser beam, mm
μ	absolute viscosity, $kg/m/\sec$
θ	angle, rad
ρ	fluid density, kg/m^3
ω_z	vorticity in the z-direction ($\omega_z = \frac{\partial V}{\partial x} - \frac{\partial U}{\partial y}$), $\sec^{-1}$

Acknowledgement

The authors would like to thank Ministry of Science and Technology (MOST) for providing financial support.

References

[1] A. C. Trupp and R. S. Azad, The Structure of Turbulent Flow in Triangular Array Rod Bundles, *Nuclear Engineering and Design*, 32, pp.47-84, 1975.

[2] S. Neti, R. Eichhorn and O. J. Hahn, Laser Doppler Measurements of Flow in a Rod Bundle, *Nuclear Engineering and Design*, 74, pp.105-116, 1982.

[3] V. Vonka, Measurement of Secondary Flow Vortices in A Rod Bundle, *Nuclear Engineering and Design*, 106, pp.191-207, 1988.

[4] D. S. Rowe and B. M. Johnson, Implications Concerning Rod Bundle Cross-flow Mixing Based On Measurements of Turbulent Flow Structure, *International Journal of Heat and Mass Transfer*, Vol. 17, pp407-419, 1974.

[5] K. Rehme, On the Development of Turbulent Flow in Wall Sub-channels of a Rod Bundle, *Nuclear Technology*, Vol. 77, pp331-342, 1987.

[6] S. K. Yang and M. K. Chung, Turbulent Flow through Spacer Grids in Rod Bundles, *Journal of Fluids Engineering, Transactions of the ASME*, Vol. 120, pp.786-791, 1998.

[7] Z. Karoutas, C. Y. Gu and B. Scholin, 3-D Flow Analyses for Design of Nuclear Fuel Spacer, *Proceedings of the 7th International Meeting on Nuclear Reactor Thermal-Hydraulics*, New York, September 10-15, Vol. 4, pp.3153-3174, 1995.

[8] L. D. Smith, III, M. E. Conner, B. Liu, M. B. Dzodzo, D. V. Paramonov, D. E. Beasley, H. M. Langford and M. V. Holloway, Benchmarking Computational Fluid Dynamics for Application to PWR Fuel, *Proceedings of 10th International Conference on Nuclear Engineering*, Arlington, VA, April 14-18, ICONE10-22475, 2002.